Controlled van der Waals Heteroepitaxy of InAs Nanowires on Carbon Honeycomb Lattices

Young Joon Hong* **and Takashi Fukui***

Research Center for Integrated Quantum Electronics (RCIQE) & Graduate School of Information Science and Technology, Hokkaido University, Sapporo 060-8628, Japan

ABSTRACT We report on unconventional, noncovalent heteroepitaxy of vertical indium arsenide (InAs) nanowires on thin graphitic films in terms of van der Waals (VDW) interactions. Nearly coherent in-plane lattice matching (misfit of 0.49%) between InAs and the graphitic surface plays a critical role in the epitaxial formation of vertical InAs nanowires on graphitic substrates. Otherwise, gallium arsenide (misfit of −6.22%) is grown to be island morphologies. Cross-sectional transmission electron microscopy analyses show that 1−2 monomolecular layer ledges or kinks facilitate heterogeneous nucleation of InAs on nonwetting graphitic surfaces, forming the nuclei and promoting the subsequent nanowire growth with strong VDW interactions at the heterojunction. We further demonstrate the controlled VDW epitaxy method for high-yield and uniform InAs nanowire arrays on honeycomb carbon surface utilizing substrate surface etching and patterning techniques. Our work opens a new platform for the III−arsenide/graphene hybrid junction electronics and optoelectronics.

KEYWORDS: van der Waals epitaxy · graphene · graphite · selective-area growth · InAs · nanowire

Paradigm shift from rigid single-crystalline silicon (Si) substrates to flexible ultrathin graphene layers has opened the floodgates for wearable, lightweight, transparent, and transferable electronic and optoelectronic devices.[1−7] This emerging substrate material, graphene or thin graphitic layer, has recently been attracting much attention, owing to its excellent electrical,[8−12] mechanical,[2,4,13] and transparent properties[14−16] as well as its large scalability.[2,11,17,18] Since the honeycomb crystal lattices of two-dimensional carbon sheets can be structurally compatible with many semiconductors of zinc blende, wurtzite, and diamond crystal structures, various semiconductors fabricated epitaxially on graphitic films can provide highly significant hybrid junctions for diverse device applications.[3,4] Nevertheless, problems associated with chemical stability of sp^2-bonded carbon atoms make it difficult to deposit various inorganic materials on graphitic layers with cohesive bonds; only a few nanomaterials including oxide semiconductors,[19−21] chalcogenides,[22] and metals[23] have thus far been successfully deposited directly on graphene materials, and the critical factors leading to the heteroepitaxy of those inorganic materials have yet to be well-established. Here, we present the critical leading factors of nucleation and growth for the heteroepitaxy of vertical indium arsenide (InAs) nanowire arrays on honeycomb carbon surface in terms of van der Waals (VDW) epitaxy. We further demonstrate the selective-area VDW heteroepitaxy for high-yield and uniform InAs nanowire arrays on graphitic substrates utilizing surface etching and substrate patterning techniques, representing a promising method for the controlled VDW heteroepitaxy.

Unconventional, noncovalent heteroepitaxy, so-called VDW heteroepitaxy, has been demonstrated by Koma *et al.* for the first time.[24] Typically, heteroepitaxial structures are grown on the substrate surface with unoccupied chemical (dangling) bonds that promote a consecutive "adatom−nucleation−growth" process to form the covalent bonding.[25] Without the surface dangling bonds of substrates, the VDW interaction, that is a universal interatomic or intermolecular force, drives the heteroepitaxy process for the energy minimizations. Importantly, since this weakly bound heterojunction (across the VDW gap) can effectively release the interfacial stress caused by lattice misfit of the heteroepitaxy, the VDW heteroepitaxy significantly improves the quality of deposited films whose feature is single-crystalline with suppressed threading defects or dislocations.[26] Although the VDW heteroepitaxy has been recognized as an important deposition method because of such advantages, only a few limited materials including layered inorganic sheets[22] or polymers[27] have been prepared on the graphitic substrates by the VDW heteroepitaxy.

RESULTS AND DISCUSSION

The basic approach for fabricating InAs nanowires on carbon honeycomb lattices is utilizing catalyst-free metal−organic

* Address correspondence to yjhong@rciqe.hokudai.ac.jp, fukui@rciqe.hokudai.ac.jp.

Received for review July 11, 2011 and accepted August 14, 2011.

Published online August 15, 2011
10.1021/nn2025786

vapor-phase epitaxy (MOVPE) and employing thin graphitic films (or graphene films) which are mechanically exfoliated from highly oriented pyrolytic graphite (HOPG). The thin graphitic films were transferred onto silicon dioxide (SiO_2)-coated Si substrates and were processed by oxygen reactive ion etching (O_2 RIE) to artificially form monomolecular layer (ML) ledges or kinks on the graphitic surface. After the O_2 plasma dry etching, the graphitic substrates were thermally cleaned under hydrogen (H_2) ambient at 600−650 °C to remove the oxygen or hydroxide adsorbates formed on the surface of the graphitic films. The InAs nanowires were then grown on the graphitic films with neither additional seed nor buffer layers.

InAs Nanostructures Grown on Thin Graphitic Films. Scanning electron microscopy (SEM) images of Figure 1a−c present the general morphologies of InAs nanowires grown on graphitic films etched by O_2 RIE for 5 s. The low-magnification image shows that all the nanowires were grown perpendicular to the graphitic layers with a uniform diameter distribution (Figure 1a): the mean diameter, height, and number density of InAs nanowire arrays grown for 20 min were measured to be 42 ± 16 nm, 0.8 ± 0.4 μm, and ≈6 × 10^8 cm^{-2}, respectively (± sign denotes the standard deviation). The vertically well-aligned InAs nanowires exhibited no tapering along the entire length of nanowires, as shown in Figure 1b, due to the well-optimized MOVPE condition for unidirectional growth of InAs nanowires.[28] The high-magnification SEM image of Figure 1b shows, however, that not only nanowires but also islands were concurrently formed on the graphitic surface. The typical size of InAs islands was approximately in the range of 50−200 nm, and the islands had hexagonal, triangular, rhombic, and even more complicated symmetries in shape, whereas all of the nanowires exhibited the same hexagonal prismatic morphology (inset in Figure 1b). Remarkably, the neighboring nanowires and islands had an identical hexagonal in-plane alignment (marked by arrows in Figure 1c) within a single domain of the graphitic layers, presumably due to the heteroepitaxial relationship between InAs and carbon honeycomb lattice. It is noteworthy that single-layer and multilayer graphenes also yielded vertically well-aligned InAs nanowires.

Without the surface etching of graphitic substrates by O_2 RIE, in contrast to the above result, freshly cleaved graphitic substrates mostly yield high-density InAs nanoislands (line number density of ~2.9 × 10^4 cm^{-1}) along the naturally formed step-edges of graphitic films, as marked with wedges in peripheries of Figure 1d,e. The heights of step-edges were measured to be ~0.4−2 nm by atomic force microscopy (AFM), corresponding to a single to several ML ledge (inset of Figure 1d). This indicates that such atomically thin ledges play an important role in the formation of high-density InAs nanoislands. Interestingly, as seen in

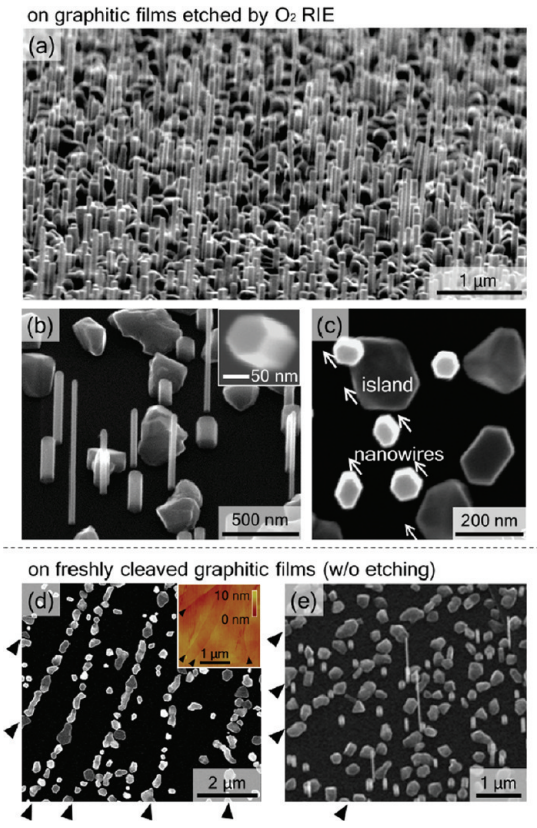

Figure 1. InAs nanostructures grown on thin graphitic films. (a−c) SEM images of vertically well-aligned InAs nanowires grown on graphitic films etched by O_2 RIE, taken at (a) 60° tilt view, (b) high-magnification 45° tilt view, and (c) top view. The inset in (b) is a top-view SEM image of a single InAs nanowire. The arrows in (c) signify that neighboring InAs nanowires have the same in-plane ordering in a six-fold rotational symmetry. (d,e) SEM images of InAs nanostructures grown on non-etched graphitic films, taken at (d) top view and (e) 45° tilt view. Inset in (d) is a surface topographic image of bare graphitic films scanned by AFM. The wedges in peripheries of (d) and (e) indicate the cleaved step-edges of graphitic layers, showing that the InAs nanoislands were mostly yielded specifically along the step-edges of graphitic substrates under the optimized nanowire growth condition.

Figure 1e, only a small number of nanowires were mostly formed in the flat terrace with a number density of ≈9 × 10^7 cm^{-2}. This value is much less than that of the islands (≈3 × 10^8 cm^{-2}) by an order of magnitude. The number density of InAs nanowires was increased by use of the etched graphitic substrates.

van der Waals Heteroepitaxy of Vertical InAs Nanowires on Graphitic Films Investigated by TEM. To explore the heteroepitaxial formation of vertical InAs nanowires on carbon honeycomb lattices, the microstructure and epitaxial relationship of InAs nanowires and thin graphitic films were examined by cross-sectional transmission electron microscopic (TEM) analyses. Figure 2a displays the cross-sectional micrograph of vertical InAs nanowires and islands formed on the graphitic layers (the graphitic layers were etched by O_2 RIE for 5 s prior to the MOVPE growth). Each nanowire exhibited an atomically flat tip morphologies (left inset in Figure 2a)

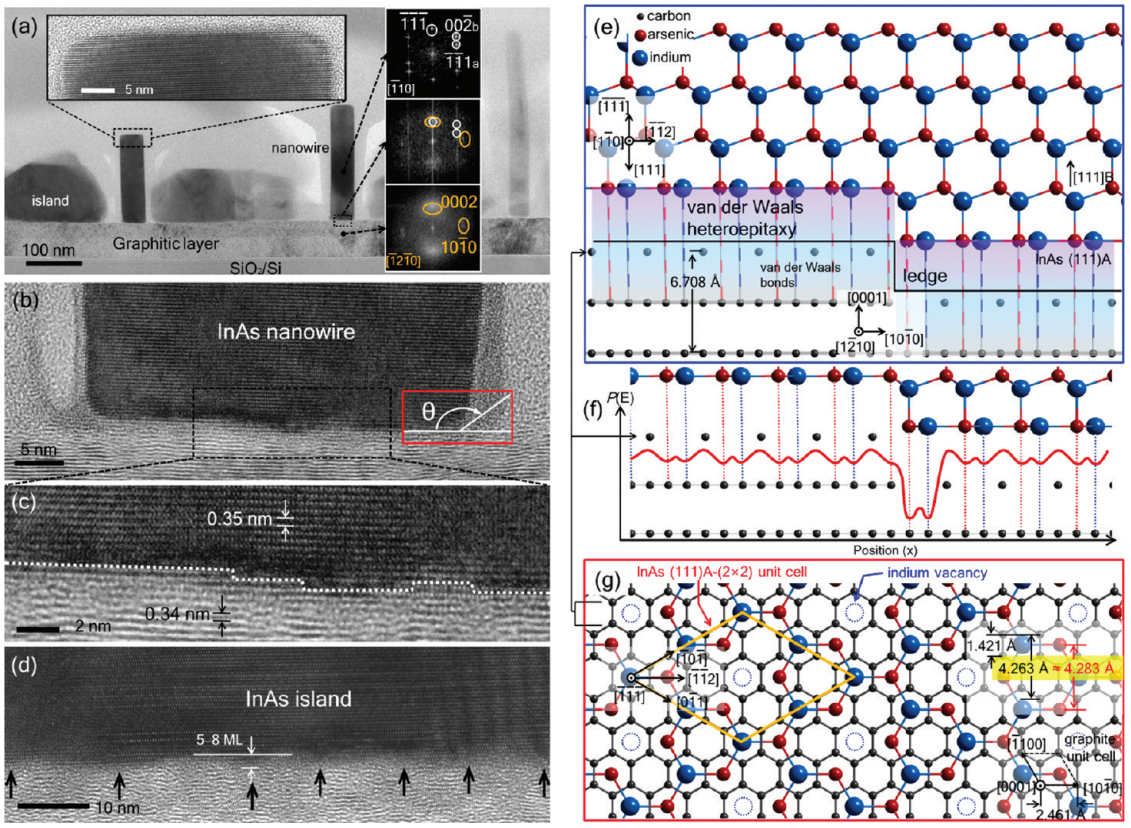

Figure 2. VDW heteroepitaxy of InAs nanowires on honeycomb carbon surface. (a) Cross-sectional TEM image of InAs nanowires and islands grown on graphitic films. Left inset in (a) is the TEM image taken around the nanowire tip showing the flat top surface. Right insets in (a) are the selected area diffraction patterns of the InAs nanowire (top panel), the interface of InAs and graphitic layer (middle panel), and the graphitic layer (bottom panel), obtained through the FFT process. (b) TEM image showing the interface of InAs nanowire and graphitic layers. The red box in (b) exhibits an obtuse contact angle between InAs and graphitic layer, implying the nonwetting graphitic surface. (c) High-resolution TEM image of the enclosed area in (b), showing the 1−2 ML ledges of graphitic layer are underneath the nanowire bottom. These ML ledges provide the heterogeneous nucleation site for the nanowire growth. The lattice spacings between adjacent planes in the nanowire and graphitic layer regions were measured to be 0.35 and 0.34 nm, corresponding to the *d* spacings of InAs (111) and graphite (0002) planes, respectively. (d) TEM image showing the interface of InAs island and graphitic layers. The arrows in (d) present very rough graphitic surface with high-density ledge grooves. (e−g) Schematic representations of the atomic configuration model for the VDW heteroepitaxy of InAs nanowires on carbon honeycomb lattices. (e) Schematic viewed along the InAs ⟨1̄10⟩ zone axis. (f) Schematic plot of the potential energy for the van der Waals heteroepitaxy of InAs on graphitic layers as a function of position on the graphitic surface. (g) Atomic configuration model showing how indium and arsenic atoms occupy their positions on the honeycomb carbon surface for the van der Waals heteroepitaxy.

and a fairly uniform diameter along the entire length, owing to the layer-by-layer growth with the inhibited radial deposition. Right inset panels in Figure 2a are the selected area diffraction patterns obtained from the InAs nanowire (top panel), the interface of nanowire/graphitic layers (middle panel), and the graphitic layer underneath the nanowire (bottom panel) by fast Fourier transform (FFT) process of the high-resolution lattice images, indicating that the zinc blende InAs nanowire grew along the [$\bar{1}\bar{1}\bar{1}$] orientation perpendicular to the graphite(0001) surface with a strong in-plane heteroepitaxial relationship of the InAs($\bar{1}\bar{1}\bar{1}$)[$\bar{1}\bar{1}2$]‖ graphite(0001)[$10\bar{1}0$].

The interfaces of InAs nanowires and islands formed on graphitic substrates were investigated by high-resolution TEM. The high-resolution micrographs reveal that the nanowires were grown upon the surface ledges with 1−2 ML depth of the graphitic layers (Figure 2b,c), whereas high-density surface grooves with 5−8 ML depth (line number density of ~7 × 10^5 cm^{-1}) were observed at the entire bottom of InAs islands (Figure 2d), implying that the 1−2 ML ledges provide a preferential nucleation site for nanowire formation and rough graphitic surface contributes to dense InAs nuclei that coalesce sufficiently to form the island morphology. These are analogous to the formation of InAs nanowire on the flat surface; the formation of islands along the step-edges is composed of continuous ledges or kinks (Figure 1d).

Meanwhile, we observed the obtuse contact angle (denoted as "θ" in red boxed area of Figure 2b) of InAs nanowire on the graphitic surface, due to the nonwettability of InAs on the hydrophobic graphitic surface. The hydrophobicity of graphite is the result of nondangling bonding surface.[29] The high surface tension between InAs and graphitic surface (by Young's equation)

makes a small contact area with the large obtuse contact angle. This small contact area determines the critical coalescence size of InAs on the nonwetting graphitic surface, which leads to the diameter-limited growth forming the nanowires. This nonwetting feature of InAs on graphitic surface is quite distinguished from the homoepitaxy of InAs nanowires on InAs(111)B substrate with the self-formed islands of a very small acute contact angle at the bottom of nanowires.[30]

For the nucleation of InAs on the nonwetting carbon honeycomb lattices, the structural imperfections of the graphitic surface, such as kinks or ledges, provide energetically favorable nucleation sites. These ledges do not provide chemical bonds because of the stable hydrogenation[31] during the MOVPE process with H_2 carrier gas (typical C−H bonding energy is 4.3 eV with bond length of 1.09 Å). However, the ledges or kinks still offer deep potential wells owing to their infinitesimal radius of curvature, as schematically depicted in Figure 2f. The deep potential well drives the diffusion and absorption of precursors toward the ledges or kinks,[32] and the long residential time of precursors around the ledges or kinks enhances the impingement of adatoms for the high nucleation probability. This overcomes the chemically stable, nonwetting graphitic surface and enables the heterogeneous nucleation of InAs on the carbon honeycomb surface.

In general, a significant driving force for heteroepitaxy is the minimization of substantial energy through a process where the dangling bonds of the substrate surface form the strong chemical bonds with the deposited materials. However, since the sp^2-bonded honeycomb carbon surface of graphite and graphene has no dangling bonds, the epitaxy of InAs nanowire on graphitic films is definitely distinct from the conventional heteroepitaxy. Hence, the driving force for the heteroepitaxy of InAs nanostructures on graphitic films is the VDW interactions, resulting in noncovalent VDW heteroepitaxy. We note that the heteroepitaxy of InAs nanowires on graphitic layers is classified into quasi-VDW epitaxy in accordance with the established criterion.[33] Previously, oxide nanomaterials have been fabricated on graphitic or graphene films by electrodeposition,[23] aqueous solution synthesis,[20] and catalyst-free MOVPE,[19] and those methods basically require either water- or oxygen-based ambient conditions for growing the oxides. Thus, oxidation of graphene surface is inevitable. A computational simulation, studied by Choi *et al.*, demonstrated the chemical bonding between the zinc oxide (ZnO) and graphene layer, verifying the covalent heterojunction.[21] The noncovalent heteroepitaxy of InAs on the hydrogenated graphitic films is, therefore, quite distinct from the chemically bonded heteroepitaxy of oxide materials on graphene.

The VDW heteroepitaxy of vertical InAs nanowire arrays on the graphitic films is strongly related to in-plane lattice matching between InAs and carbon honeycomb lattice. As presented in Figure 2g (also Figures S3 and S4 in Supporting Information), the distance of the nearest neighbor carbon honeycombs along $\langle 1\bar{2}10\rangle$ is 4.263 Å which corresponds to three times the distance of the nearest carbon atoms (=1.421 Å) in the graphitic layer (a = 2.461 Å, c = 6.708 Å for graphite). Note that this honeycomb−honeycomb distance of 4.263 Å has only a small misfit of 0.49% with the nearest arsenic−arsenic (or indium−indium) distance of $a/\sqrt{2}$ = 4.284 Å ($a = c$ = 6.058 Å for zinc blende InAs) (Figure S3 in Supporting Information). Hence, it is energetically favorable when the primitive lattices of InAs fix up their positions upon the hollows of each carbon honeycomb along the lattice-matched $\langle 1\bar{2}10\rangle$ of c-plane graphitic surface, as depicted in Figure 2g. This energy saving contributes to the heteroepitaxy of InAs$(\bar{1}\bar{1}\bar{1})[1\bar{1}0]\|$graphite$(0001)[1\bar{2}10]$; InAs$(\bar{1}\bar{1}\bar{1})[\bar{1}\bar{1}2]\|$graphite$(0001)[10\bar{1}0]$. Meanwhile, we have previously demonstrated vertical InAs nanowires grow along [111]B orientation,[28] thus it has been presumed that the bottom layer of nanowire consists of (111)A. The adatom layer of the InAs(111)A basal plane, weakly bound to the graphitic surface, must undergo a reconstruction process at the initial growth stage. Considering the previous theoretical and empirical studies on the InAs(111)A surface,[34,35] it is reasonably expected that the initial InAs(111)A basal layer forms extremely flat honeycomb lattice surface with an indium vacancy in each InAs(111)A−2 × 2 unit cell (Figure 2g and Figure S3 in Supporting Information). Because the indium and arsenic adatoms are at the same distance from the graphitic surface (Figure 2e,f), such reconstructed flattened InAs(111)A bottom layer with a small lattice misfit of 0.49% maximizes the VDW bonding forces. The maximized cohesive force enables the heteroepitaxial formation of vertical nanowire morphology, even though the VDW bonding energy is much smaller than that of covalent bond (typically a few electronvolts) by 2 or 3 orders of magnitude. More importantly, no threading dislocations were observed at the VDW heterointerfaces presumably due to the stress-relaxed epitaxy of InAs nanostructures with the weakly bound VDW attractions and the small in-plane lattice mismatch between InAs(111) and graphite(0001).

In order to clarify the role of in-plane lattice matching in the VDW heteroepitaxy for vertical nanowire arrays, well-optimized MOVPE growth condition for gallium arsenide (GaAs) nanowires was applied to the graphitic substrates in a same manner. According to the previous theoretical calculations for metal adatom adsorption on graphene, the energetic and structural properties of gallium and indium adatoms on graphene are analogous to each other.[36] Hence, there is

a possibility of formation of vertical GaAs nanowires on the graphitic layer. However, the graphitic surface only yielded GaAs island morphologies mostly along the step-edges of the graphitic layers (Figure S1 in Supporting Information) under the optimized GaAs nanowire growth condition.[37] The neighboring GaAs islands did not exhibit the in-plane alignment, implying non-epitaxial deposition of GaAs on graphite. The non-epitaxial formation of GaAs island morphologies can be attributed to the large lattice mismatch of −6.22% between the arsenic−arsenic distance in GaAs and the honeycomb−honeycomb distance along $\langle 1\bar{2}10 \rangle$ in graphite. This observation supports the argument that the nearly coherent lattice matching is very crucial in the VDW heteroepitaxy for vertical nanowire formation.

To date, the VDW heteroepitaxy has mostly yielded two-dimensional ultrathin chalcogenide lamellar structures[22,38] or molecular layers.[39] In those cases, the VDW adhesion is strong enough because of high junction area-to-volume ratio, so that the large lattice misfit does not trouble the epitaxy. However, where the heterojunction area diminishes into the nanoscale for three-dimensional nanoarchitectures, the lattice coherency becomes critical for both the epitaxial formation and adhesive mechanical support. Therefore, the maximized VDW interaction per unit area at the heterojunction is important to design a new VDW epitaxy of nanoscale inorganic materials on graphitic substrates.

Surface Engineering of Graphitic Films for Density-Controlled VDW Heteroepitaxy of InAs Nanowires. Motivated by the observation that the surface roughness of graphitic films determines the morphology of either nanowire or island, we investigated the effect of etching of graphitic substrates on the controlled VDW growth of InAs nanowires for obtaining high-density nanowire arrays. To control the surface roughness of graphitic layers, O_2 RIE time was varied. Figure 3a presents the plots of root-mean-square (rms) roughness of graphitic layers as a function of O_2 RIE time, characterized by AFM. The rms roughness of entire surface of pristine graphitic flakes, including the step-edges, was estimated to be 0.33 ± 0.11 nm (solid squares in Figure 3a), while the rms roughness in a single terrace was not measurable within a detection limit of AFM, indicating the extremely smooth surface of non-etched graphitic terrace (empty circles in Figure 3a). The O_2 RIE increased the rms roughness of entire graphitic surface as well as that of the terrace with an equivalent increasing rate of ∼0.3−0.4 Å s^{-1}, indicating that the etching roughens mostly the terraces. Noticeably, the rms roughness of the terrace was controlled in a ML level so that the method can be easily applied to growth of high-density InAs nanowire arrays. Figure 3b exhibits that the number densities of InAs nanowire (solid circles) and island (empty triangles) on graphitic layers were changed by the O_2 RIE time of the substrates. The

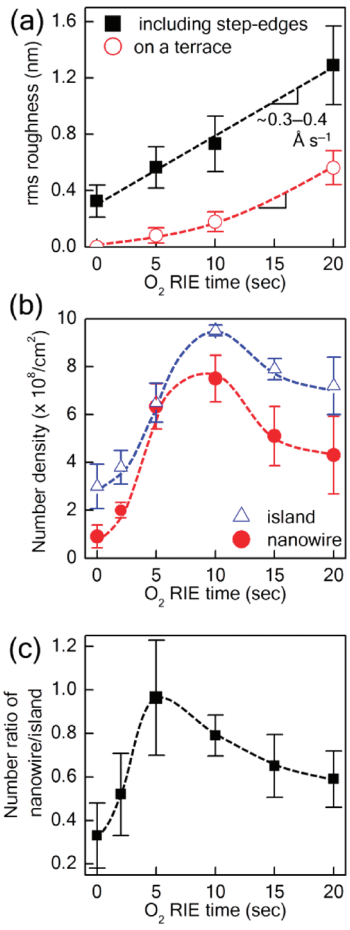

Figure 3. Surface engineering of graphitic substrates for obtaining high-yield and high-density InAs nanowire arrays. (a) Plots of rms roughness of graphitic films etched by O_2 RIE as a function of the RIE time, measured over the entire surface of graphitic films including step-edges (black solid squares) and within a terrace surface (red empty circles). (b) Plots of number density of InAs nanowires (red solid circles) and islands (blue empty triangles) fabricated on graphitic films as a function of O_2 RIE time of graphitic substrates. (c) Plot of number ratio of nanowire to island formed on the graphitic films *versus* the O_2 RIE time of the substrates. All error bars denote the standard deviations.

number density of nanowires was increased significantly from (0.9 ± 0.5) × 10^8 to (7.5 ± 1.0) × 10^8 cm^{-2}, while that of islands from (3.0 ± 0.9) × 10^8 to (9.5 ± 0.2) × 10^8 cm^{-2} with increasing the O_2 RIE time from 0 to 10 s, implying that the roughening of the terrace promotes more considerably the nanowire growth than the island formation. However, further increase of the O_2 RIE time over 10 s gradually decreased the number density of both InAs nanowires and islands presumably because the highly rough graphitic surface inhibits the VDW epitaxy. We plotted the number ratio of nanowire to island as a function of O_2 RIE time (Figure 3c). Since the number density of the nanowires increases greater than that of the islands with increasing the O_2 RIE time, the number ratio of nanowire to island was increased from 0.33 ± 0.15 to 0.96 ± 0.26 by extending the RIE time up to 5 s. However, further increase in RIE time

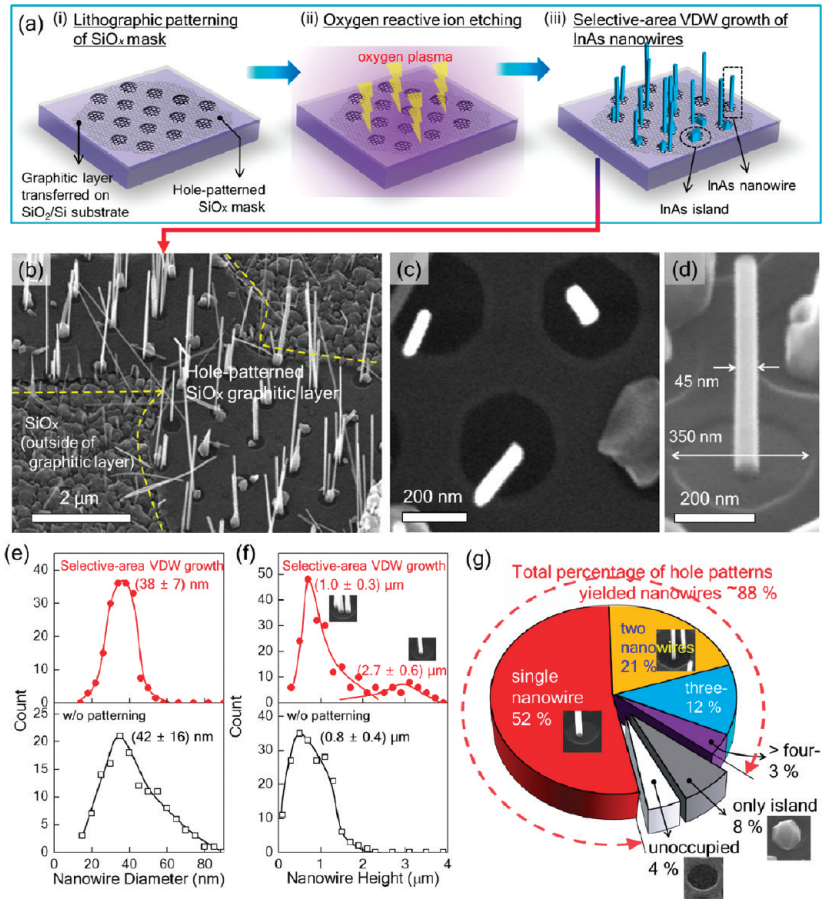

Figure 4. Selective-area van der Waals heteroepitaxial growth of InAs nanowire arrays on patterned graphitic layers. (a) Schematics of the fabrication process for selective-area VDW growth of InAs nanowires on patterned graphitic layers. (b,c) SEM images of InAs nanowire arrays grown on hole-patterned graphitic layers after the process of (iii) in (a). The images of (b) and (c) are taken at bird's eye and top view, respectively. (d) High-magnification tilt view SEM image of a single InAs nanowire grown in a hole pattern on thin graphitic layers, showing that the diameter of nanowire was not determined by the hole size. Histograms of (e) diameter and (f) height of nanowire arrays grown on patterned graphitic layers by selective-area VDW heteroepitaxy (plotted with red solid circles in upper parts) and on nonpatterned graphitic layers (plotted with black empty squares in lower parts) for 20 min nanowire growth. Mean and standard deviation values were given in each plot. (g) Pie chart summarizing the percentage of hole patterns yielded InAs nanowires and islands after selective-area VDW growth.

gradually decreased the number ratio. In addition to the statistical information, the rms roughness of the graphitic layer influenced the vertical alignment of InAs nanowires; rough graphitic surface produced inclined nanowires (Figure S2 in Supporting Information). Therefore, the surface engineering of graphitic substrates is of importance for achieving the controlled VDW growth of InAs nanowires.

Selective-Area VDW Heteroepitaxy of InAs Nanowires on Graphitic Films. Both high-yield growth of vertical nanowire arrays and control of their spatial arrangement are necessary for highly integrated, addressable electronic[40,41] and optoelectronic device fabrication.[42,43] The approach for high-yield and position-controlled InAs nanowire arrays is the selective-area VDW growth using a patterned mask layer. Since the mask layer covers the naturally formed step-edges of graphitic films, it can suppress effectively the unwanted island formations. First, thin graphitic layers were transferred onto the foreign SiO_2/Si substrates, followed by deposition of SiO_x mask layer, chosen as the RIE resist and the growth mask material. Hole patterns of the mask were prepared by electron-beam lithography and selective etching of the SiO_x mask, as depicted in process (i) of Figure 4a. Then, the O_2 RIE method was utilized to etch the predefined area of graphitic layer through the hole opening of mask layer (process (ii) in Figure 4a).

The selective-area dry etching contributed to the selective-area VDW growth of InAs nanowires. Figure 4b,c is the SEM images after the selective-area VDW growth shown in process (iii) of Figure 4a, displaying that the InAs nanowires were selectively grown only on the hole-patterned graphitic layer. Interestingly, as shown in Figure 4d, the diameter of nanowires was not determined by patterned hole diameter, dissimilar to the selective-area growth of InAs nanowires on Si or III−V substrates.[28] This hole-size-independent growth behavior can be elucidated by diameter-limited growth on the nonwetting graphitic surface, as mentioned in above. The selective-area VDW growth,

however, enhanced the diameter uniformity as displayed in Figure 4e; the diameter of the selectively grown InAs nanowires was measured to be 38 ± 7 nm (top panel) whose distribution value is more uniform than that of the InAs nanowires grown on nonpatterned graphitic surfaces (bottom panel). The enhanced narrow distribution of the nanowire diameter is attributed to the regular surface collection area of patterned selective growth.[44] Moreover, the selective-area VDW growth increased nanowire growth rate and uniformity (Figure 4f). Since the selective-area growth reduces effectively the precursor waste by preventing the unwanted formation of nanoisland on undefined areas, the mean height of nanowire was increased from 0.8 ± 0.4 to 1.3 ± 0.6 μm. Interestingly, the nanowire height histogram (fabricated by selective-area growth) exhibited bimodal distributions (top panel in Figure 4f). The histogram curve of the smaller nanowire height with a mean value of 1.0 ± 0.3 μm is attributed to plural nanowires formed in a hole pattern, whereas that of taller nanowire height with the mean value of 2.7 ± 0.6 μm is from a single nanowire grown in each hole pattern. These bimodal nanowire height distributions can be easily explained by the precursor consumption in a surface collection area. The plural nanowires in a hole divide their supplied precursors, while a single nanowire in a hole consumes all of the supplied precursors in a surface collection area by itself, resulting in the bimodal height distributions. We plotted the yield of selective-area VDW growth of InAs nanowires with a pie chart in Figure 4g. The portion of holes yielded InAs nanowire was measured to be approximately 88% (left column), while the 8 and 4% hole patterns yielded only the island and none, respectively, verifying the high-yield selective-area VDW epitaxy of InAs nanowires. We believe that further optimization will enhance the nanowire yield close to nearly 100%.

CONCLUSIONS

We have demonstrated the VDW heteroepitaxy and the critical leading factors for the fabrication of inorganic nanomaterials on graphitic substrates. The in-plane lattice coherency and controlled surface atomic layer ledge of graphitic substrates contributed to the VDW heteroepitaxial formation of vertical InAs nanowire arrays. By combining the designed procedures, such as dry etching and substrate patterning, the controlled, selective-area VDW heteroepitaxy of InAs nanowire arrays on the graphitic films was accomplished. All of the features of the VDW heteroepitaxy, which produces high-yield, very uniform vertical nanowires with a controlled manner, readily offer significant opportunities for fabricating various semiconductor devices on carbon honeycomb lattices.

METHODS

Preparation of Substrates. The graphitic films including thin graphite flakes and few-layer graphene sheets were transferred onto the SiO_2/Si substrates using a simple mechanical exfoliation technique (so-called scotch tape method).[8] The mother material of the transferred graphitic layers was HOPG (Mikromasch ZYA1 grade, chip size of 1 mm × 10 mm × 10 mm) with a mosaic spread of 0.4 ± 0.1° and lateral grain sizes of typically up to 10 μm. After the transfer process, the substrates were immersed in acetone for over 7 days and cleaned with nitric acid (NH_4Cl) to remove the organic residues. Immediately after the organic cleaning process, the substrates were annealed at 800 °C and 1 atm for 10 min under the nitrogen ambient. For the selective-area VDW growth, a 20 nm thick SiO_x mask layer was deposited on the whole surface of graphitic layer-transferred substrate by sputtering method (Anelva L-250S-FH), followed by electron-beam lithographic patterning (Jeol JBX-6300FS). In order to artificially form the ML ledges or kinks on graphitic layers, O_2 RIE technique (Samco RIE-10NRV) was utilized as a dry etching method.[45,46] To control the roughness of graphitic layer, the RIE time was varied under the fixed O_2 flow rate of 20 sccm and the applied radio frequency power of 100 W at reactor pressure of 150 mTorr.

Growth Procedures. The VDW heteroepitaxy of InAs nanowires was performed using a low-pressure horizontal reactor MOVPE. High-purity H_2 was employed as a carrier gas, purified through palladium membrane. The total flow rate of the gases was maintained at 5.75 sLm (standard liter per minute) during MOVPE growth process. For the growth of the InAs nanowires, trimethylindium (TMIn) and 5% arsine (AsH_3) diluted with H_2 were used as precursors with typical partial pressures of 4.9 × 10^{-7} and 1.3 × 10^{-4} atm, respectively. Prior to the growth, thermal cleaning was carried out at 600−650 °C for 10 min under the H_2 ambient to remove the oxygen or hydroxide adsorbates formed on the graphitic surface. Immediately after the thermal cleaning, AsH_3 purge procedure was performed at 410 °C under the partial AsH_3 pressure of 2.5 × 10^{-4} atm. For the enhanced nucleation and growth of InAs, the flow-rate-modulated epitaxy (FME) mode was performed with repetitive FME cycles during temperature ramping from 410 to 560 °C.[28] Subsequently, InAs growth was performed at 560 °C for 20 min with a fixed reactor pressure of 76 Torr.

The GaAs was grown at 760 °C for 40 min. The partial pressure of trimethylgallium (TMGa) was 1.0 × 10^{-6}, and that of AsH_3 was 2.5 × 10^{-4} atm. For the enhanced growth of GaAs, the optimized FME mode was utilized.[37]

Characterizations. Morphological and microstructural analyses were performed using SEM (Hitachi S-4100) and high-resolution TEM (Hitachi H-9000UHR), respectively. For cross-sectional TEM imaging and electron diffraction analysis, samples were milled with 5−30 keV accelerated gallium ions using a focused ion beam machine (FIB; Hitachi FB-2100 m and FEI STRATA DB235). Argon ion milling machine (Gatan 600N Duomill) was also utilized to mill the cross-sectional sample. The acceleration voltage for the TEM inspection was in the range of 100−300 keV. The incident electron beam was directed along the InAs $\langle 1\bar{1}0 \rangle$ orientation to define the crystal structure of InAs nanowires. The rms roughness of graphitic layers was measured on 5 μm × 5 μm by AFM (Veeco Nanoscope Multimode SPM).

Acknowledgment. The authors thank Prof. Motohisa, Prof. Hara, and Prof. Koga at Hokkaido University, and Dr. Hiruma at Hitachi Co. for their valuable comments and discussions. We also acknowledge Dr. Tomioka, Mr. Yoshimura, and Mr. Ikejiri for their support in MOVPE experiments. This work was financially supported by Grant-in-Aid for Specially Promoted Research (No. 18002003) from Japan Society for the Promotion of Science (JSPS).

Supporting Information Available: GaAs nanostructures grown on thin graphitic films (S1); the effect of roughness of graphitic substrates on vertical alignment of InAs nanowires (S2); schematics of atomic configurations for the VDW heteroepitaxy of InAs on graphitic films (S3 and S4). This material is available free of charge *via* the Internet at http://pubs.acs.org.

REFERENCES AND NOTES

1. Eda, G.; Fanchini, G.; Chhowalla, M. Large-Area Ultrathin Films of Reduced Graphene Oxide as a Transparent and Flexible Electronic Material. *Nat. Nanotechnol.* **2008**, *3*, 270–274.
2. Bae, S.; Kim, H.; Lee, Y.; Xu, X.; Park, J.-S.; Zheng, Y.; Balakrishnan, J.; Lei, T.; Kim, H. R.; Song, Y. I.; *et al.* Roll-to-Roll Production of 30-Inch Graphene Films for Transparent Electrodes. *Nat. Nanotechnol.* **2010**, *5*, 574–578.
3. Chung, K.; Lee, C.-H.; Yi, G.-C. Transferable GaN Layers Grown on ZnO-Coated Graphene Layers for Optoelectronic Devices. *Science* **2010**, *330*, 655–657.
4. Choi, D.; Choi, M.-Y.; Choi, W. M.; Shin, H.-J.; Park, H.-K.; Seo, J.-S.; Park, J.; Yoon, S.-M.; Chae, S. J.; Lee, Y. H.; *et al.* Fully Rollable Transparent Nanogenerators Based on Graphene Electrodes. *Adv. Mater.* **2010**, *22*, 2187–2192.
5. Gomez De Arco, L.; Zhang, Y.; Schlender, C. W.; Ryu, K.; Thompson, M. E.; Zhou, C. Continuous, Highly Flexible, and Transparent Graphene Films by Chemical Vapor Deposition for Organic Photovoltaics. *ACS Nano* **2010**, *4*, 2865–2873.
6. Lee, D. H.; Lee, J. A.; Lee, W. J.; Kim, S. O. Flexible Field Emission of Nitrogen-Doped Carbon Nanotubes/Reduced Graphene Hybrid Films. *Small* **2011**, *7*, 95–100.
7. Ji, Y.; Lee, S.; Cho, B.; Song, S.; Lee, T. Flexible Organic Memory Devices with Multilayer Graphene Electrodes. *ACS Nano* **2011**, *5*, 5995–6000.
8. Novoselov, K. S.; Geim, A. K.; Morozov, S. V.; Jiang, D.; Zhang, Y.; Dubonos, S. V.; Grigorieva, I. V.; Firsov, A. A. Electric Field Effect in Atomically Thin Carbon Films. *Science* **2004**, *306*, 666–669.
9. Zhang, Y.; Tan, Y.-W.; Stormer, H. L.; Kim, P. Experimental Observation of the Quantum Hall Effect and Berry's Phase in Graphene. *Nature* **2005**, *438*, 201–204.
10. Ang, P. K.; Chen, W.; Wee, A. T. S.; Loh, K. P. Solution-Gated Epitaxial Graphene as pH Sensor. *J. Am. Chem. Soc.* **2008**, *130*, 14392–14393.
11. Lin, Y.-M.; Dimitrakopoulos, C.; Jenkins, K. A.; Farmer, D. B.; Chiu, H.-Y.; Grill, A.; Avouris, P. 100-GHz Transistors from Wafer-Scale Epitaxial Graphene. *Science* **2010**, *327*, 662.
12. Yoo, J. J.; Balakrishnan, K.; Huang, J.; Meunier, V.; Sumpter, B. G.; Srivastava, A.; Conway, M.; Reddy, A. L. M.; Yu, J.; Vajtai, R.; *et al.* Ultrathin Planar Graphene Supercapacitors. *Nano Lett.* **2011**, *11*, 1423–1427.
13. Lee, C.; Wei, X.; Kysar, J. W.; Hone, J. Measurement of the Elastic Properties and Intrinsic Strength of Monolayer Graphene. *Science* **2008**, *321*, 385–388.
14. Li, X.; Zhang, G.; Bai, X.; Sun, X.; Wang, X.; Wang, E.; Dai, H. Highly Conducting Graphene Sheets and Langmuir–Blodgett Films. *Nat. Nanotechnol.* **2008**, *3*, 538–542.
15. Becerril, H. A.; Mao, J.; Liu, Z.; Stoltenberg, R. M.; Bao, Z.; Chen, Y. Evaluation of Solution-Processed Reduced Graphene Oxide Films as Transparent Conductors. *ACS Nano* **2008**, *2*, 463–470.
16. Lee, J. M.; Choung, J. W.; Yi, J.; Lee, D.; Samal, M.; Yi, D. K.; Lee, C.-H.; Yi, G.-C.; Paik, U.; Rogers, J. A.; *et al.* Vertical Pillar-Superlattice Array and Graphene Hybrid Light Emitting Diodes. *Nano Lett.* **2010**, *10*, 2783–2788.
17. Li, X.; Cai, W.; An, J.; Kim, S.; Nah, J.; Yang, D.; Piner, R.; Velamakanni, A.; Jung, I.; Tutuc, E.; *et al.* Large-Area Synthesis of High-Quality and Uniform Graphene Films on Copper Foils. *Science* **2009**, *324*, 1312–1314.
18. Reina, A.; Jia, X.; Ho, J.; Nezich, D.; Son, H.; Bulović, V.; Dresselhaus, M. S.; Kong, J. Large Area, Few-Layer Graphene Films on Arbitrary Substrates by Chemical Vapor Deposition. *Nano Lett.* **2009**, *9*, 30–35.
19. Kim, Y.-J.; Lee, J. H.; Yi, G.-C. Vertically Aligned ZnO Nanostructures Grown on Graphene Layers. *Appl. Phys. Lett.* **2009**, *95*, 213101.
20. Lee, J. M.; Pyun, Y. B.; Yi, J.; Choung, J. W.; Park, W. I. ZnO Nanorod–Graphene Hybrid Architectures for Multifunctional Conductors. *J. Phys. Chem. C* **2009**, *113*, 19134–19138.
21. Choi, W. M.; Shin, K.-S.; Lee, H. S.; Choi, D.; Kim, K.; Shin, H.-J.; Yoon, S.-M.; Choi, J.-Y.; Kim, S.-W. Selective Growth of ZnO Nanorods on SiO_2/Si Substrates Using a Graphene Buffer Layer. *Nano Res.* **2011**, *4*, 440–447.
22. Dang, W.; Peng, H.; Li, H.; Wang, P.; Liu, Z. Epitaxial Heterostructures of Ultrathin Topological Insulator Nanoplate and Graphene. *Nano Lett.* **2010**, *10*, 2870–2876.
23. Zach, M. P.; Ng, K. H.; Penner, R. M. Molybdenum Nanowires by Electrodeposition. *Science* **2000**, *290*, 2120–2123.
24. Koma, A.; Sunouchi, K.; Miyajima, T. Fabrication and Characterization of Heterostructures with Subnanometer Thickness. *Microelectron. Eng.* **1984**, *2*, 129–136.
25. Ayers, J. E. *Heteroepitaxy of Semiconductors: Theory, Growth, and Characterization*; CRC Press: Boca Raton, FL, 2007.
26. Takeyama, S.; Watanabe, K.; Ichihara, M.; Suzuki, K.; Miura, N. van der Waals Epitaxial Growth of Thin BiI_3 Films on PbI_2 and CdI_2 Substrates by a Hot Wall Method. *J. Appl. Phys.* **1990**, *68*, 2735–2738.
27. Forrest, S. R.; Burrows, P. E.; Haskal, E. I.; So, F. F. Ultrahigh-Vacuum Quasiepitaxial Growth of Model van der Waals Thin Films. II. Experiment. *Phys. Rev. B* **1994**, *49*, 11309–11321.
28. Tomioka, K.; Motohisa, J.; Hara, S.; Fukui, T. Control of InAs Nanowire Growth Directions on Si. *Nano Lett.* **2008**, *8*, 3475–3480.
29. Wang, S.; Zhang, Y.; Abidi, N.; Cabrales, L. Wettability and Surface Free Energy of Graphene Films. *Langmuir* **2009**, *25*, 11078–11081.
30. Dayeh, S. A.; Yu, E. T.; Wang, D. III–V Nanowire Growth Mechanism: V/III Ratio and Temperature Effects. *Nano Lett.* **2007**, *7*, 2486–2490.
31. Meyer, J. C.; Girit, C. O.; Crommie, M. F.; Zettl, A. Imaging and Dynamics of Light Atoms and Molecules on Graphene. *Nature* **2008**, *454*, 319–322.
32. Uthaisar, C.; Barone, V. Edge Effects on the Characteristics of Li Diffusion in Graphene. *Nano Lett.* **2010**, *10*, 2838–2842.
33. Koma, A. Van der Waals Epitaxy—A New Epitaxial Growth Method for a Highly Lattice-Mismatched System. *Thin Solid Films* **1992**, *216*, 72–76.
34. Ohtake, A.; Ozeki, M.; Nakamura, J. Strain Relaxation in InAs/GaAs(111)A Heteroepitaxy. *Phys. Rev. Lett.* **2000**, *84*, 4665–4668.
35. Taguchi, A.; Kanisawa, K. Stable Reconstruction and Adsorbates of InAs(111)A Surface. *Appl. Surf. Sci.* **2006**, *252*, 5263–5266.
36. Chan, K. T.; Neaton, J. B.; Cohen, M. L. First-Principles Study of Metal Adatom Adsorption on Graphene. *Phys. Rev. B* **2008**, *77*, 235430.
37. Tomioka, K.; Kobayashi, Y.; Motohisa, J.; Hara, S.; Fukui, T. Selective-Area Growth of Vertically Aligned GaAs and GaAs/AlGaAs Core–Shell Nanowires on Si(111) Substrate. *Nanotechnology* **2009**, *20*, 145302.
38. Lang, O.; Schlaf, R.; Tomm, Y.; Pettenkofer, C.; Jaegermann, W. Single Crystalline GaSe/WSe_2 Heterointerfaces Grown by van der Waals Epitaxy. I. Growth Conditions. *J. Appl. Phys.* **1994**, *75*, 7805–7813.
39. Zhang, Y.; Forrest, S. R. Mechanisms of Quasiepitaxial Ordering at Organic Molecular Thin Film Interfaces. *Phys. Rev. Lett.* **1993**, *71*, 2765–2768.
40. Ng, H. T.; Han, J.; Yamada, T.; Nguyen, P.; Chen, Y. P.; Meyyappan, M. Single Crystal Nanowire Vertical Surround-Gate Field-Effect Transistor. *Nano Lett.* **2004**, *4*, 1247–1252.
41. Tomioka, K.; Fukui, T. Tunnel Field-Effect Transistor Using InAs Nanowire/Si Heterojunction. *Appl. Phys. Lett.* **2011**, *98*, 083114.

42. Lee, C.-H.; Yoo, J.; Hong, Y. J.; Cho, J.; Kim, Y.-J.; Jeon, S.-R.; Baek, J. H.; Yi, G.-C. GaN/$In_{1-x}Ga_xN$/GaN/ZnO Nanoarchitecture Light Emitting Diode Microarrays. *Appl. Phys. Lett.* **2009**, *94*, 213101.
43. Tomioka, K.; Motohisa, J.; Hara, S.; Hiruma, K.; Fukui, T. GaAs/AlGaAs Core Multishell Nanowire-Based Light-Emitting Diodes on Si. *Nano Lett.* **2010**, *10*, 1639–1644.
44. Jensen, L. E.; Björk, M. T.; Jeppesen, S.; Persson, A. I.; Ohlsson, B. J.; Samuelson, L. Role of Surface Diffusion in Chemical Beam Epitaxy of InAs Nanowires. *Nano Lett.* **2004**, *4*, 1961–1964.
45. Yang, R. T.; Wong, C. Mechanism of Single-Layer Graphite Oxidation: Evaluation by Electron Microscopy. *Science* **1981**, *214*, 437–438.
46. Lu, X.; Huang, H.; Nemchuk, N.; Ruoff, R. S. Patterning of Highly Oriented Pyrolytic Graphite by Oxygen Plasma Etching. *Appl. Phys. Lett.* **1999**, *75*, 193–195.